Advanced Steel Construction – Vol. 19 No. 2 (2023) 91–101
DOI:10.18057/IJASC.2023.19.2.1

EXPERIMENTAL STUDY ON CYCLIC BEHAVIOR OF BLIND-BOLT JOINT CONNECTING STEEL BEAM AND RECTANGULAR TUBE COLUMN

Guo-Qiang Li [1, 2], Yun-Han Jiang [1], Yuan-Zuo Wang [3, 4, *] and Chen Chen [1]

[1] *College of Civil Engineering, Tongji University, Shanghai, China*
[2] *National Key Lab for Disaster Reduction in Civil Engineering, Tongji University, Shanghai, China*
[3] *Key Laboratory of Urban Security and Disaster Engineering of Ministry of Education, Beijing University of Technology, Beijing, China*
[4] *Faculty of Engineering, Hokkaido University, Hokkaido, Sapporo, Japan*
** (Corresponding author: E-mail: yzwang@bjut.edu.cn)*

ABSTRACT

An experimental investigation on the cyclic behavior of the joints for steel H-shaped beams to steel rectangular tube columns using end-plate and blind bolts is conducted in this paper. The load-bearing capacity, rotation stiffness and hysteretic behavior of the joints are studied. In terms of the types of beams (pure steel beam and composite steel beam with concrete slab) and columns (pure steel rectangular tube column and concrete-filled steel rectangular tube column), a total of four different joints are tested and compared. It is found that filling concrete in rectangular tube columns can avoid the failure mode of column tube wall yielding under bending moment. Furthermore, due to the contribution of the concrete slab, the bending capacity and initial rotational stiffness of the composite steel beam-to-column joint are significantly greater than those of the pure steel beam-to-column joint under sagging or hogging moments. Under most circumstances, the joints demonstrate excellent ductility with the interstory displacement angle greater than 0.04 rad, which satisfies the requirement for resisting severe earthquakes.

ARTICLE HISTORY

Received: 20 September 2022
Revised: 16 January 2023
Accepted: 20 January 2023

KEYWORDS

Blind bolt;
Beam-to-column joint;
H-shaped beam;
Rectangular tube column;
Concrete-filled tube column;
Cyclic behavior

1. Introduction

Compared with the H-shaped column, the steel tube column with rectangular hollow section (RHS) exhibits more excellent static and seismic properties including higher strength and stiffness owing to its closed and symmetric cross-section. Previous research has shown that steel frame systems using RHS columns were usually able to not only reduce steel consumption but also improve space utilization[1]. The strength and ductility of the beam-to-column joints are critical for the application of such steel tube columns.

The most widely used method for connecting H-shaped beams to RHS columns is full welding, as illustrated in Fig. 1. Although the fully welded steel beam-to-RHS column connection possesses high bearing capacity and stiffness, it is easily fractured as observed in the 1994 Northbridge earthquake and the 1995 Kobe earthquake (Fig. 2)[2, 3]. Moreover, due to high technical requirements and slow speed in the construction of the welded joints, the full welding method no longer fulfils the requirements of assembly construction of steel structure buildings.

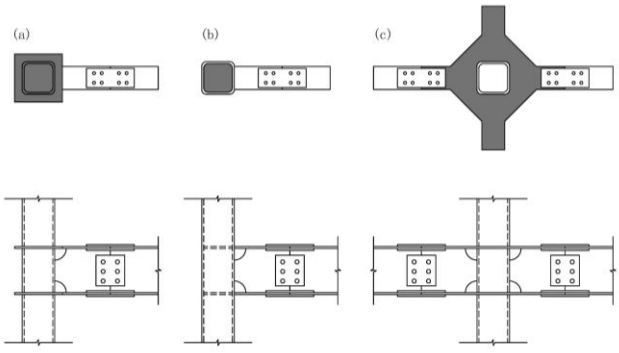

(a) through-diaphragm; (b) interior diaphragm; (c) exterior diaphragm.

Fig. 1 Typical steel beam-to-RHS column fully welded connections

(a) Northbridge earthquake[2]

(b) Kobe earthquake[3]

Fig. 2 Failure of the steel beam-to-column fully welded connections

Motivated by these incidents, bolted joints with end-plates are increasingly used to connect steel beams to columns, as shown in Fig. 3. The fracture failure of the fully welded connection can be prevented. In addition, these joints can be much more efficiently erected than those fully welded. Nevertheless, it is hard to connect H-shaped beams and RHS columns with traditional high strength bolts, which needs operation at both sides of the connected elements.

Fig. 3 Typical steel beam-to-column fully bolted connection

To solve this problem, specific blind bolts, such as Hollo-Bolt[4] and similar self-locking bolts[5, 6], as shown in Fig. 4, being able to be operated at only one side of the connected element, are proposed to replace the traditional high strength bolts. With such blind bolts, the steel beam-to-RHS column fully bolted connections can be efficiently achieved on site, as shown in Fig. 5.

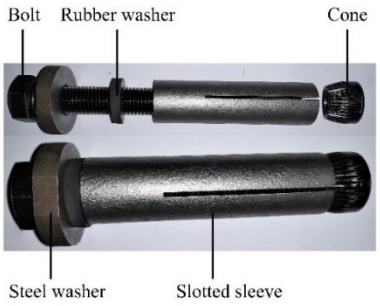

Fig. 4 Blind Bolts

Fig. 5 Steel beam-to-RHS column fully bolted connection

The joints between H-shaped steel beams and rectangular steel tubular columns using blind bolts have been extensively studied by a number of researchers that respectively analyzed the beam-to-column joints with HSBB[7, 8], Flowdrill blind bolts[9, 10], RMH blind bolts[11, 12], Hollo-bolt[13, 14] and ONESIDE Fastener blind bolts[15, 16]. These studies show that the thickness of the tube wall is an essential factor for the failure modes of the joints and the stiffness of these joints is less than those using normal high strength bolts.

In respect of filling concrete in the columns, Wang et al.[17-26] conducted static and seismic experimental investigations into H-shaped beam-to-RHS concrete-filled column end-plate connections by means of Hollo-Bolts, and Li et al.[27] completed the seismic performance tests of eight RHS concrete-filled columns and H-shaped steel beam joints connected by slip-critical blind bolts. These studies show that concrete-filled steel tubular column joints have higher initial rotational stiffness, load-bearing capacity and excellent energy dissipation capacity. Considering the effect of concrete slabs, Wang et al.[19-21] and Jiao et al.[28] studied the H-shaped steel beam with concrete floor slab and rectangular steel tube column joints using Hollo-Bolts and slip-critical blind bolts, respectively. It was found that the stiffness and bending capacity of the composite beam joints with concrete slabs are significantly increased, and the hysteretic performance of the joints was also improved.

However, in the previous studies, the failure of the beam-to-column joints with blind bolts under bending usually occurs in the joint core. This failure mode will make the wall of the rectangular steel tube column yield or even deflect out-of-plane. Unfortunately, this kind of joint failure is highly unfavorable to the vertical load-bearing capacity of the columns. To mitigate the damage of the joint zone in the columns, an end-plate yielding failure mode is introduced at the joints of steel beams to rectangular hollow section columns in this paper. Through proper design of the thickness and size of the end-plate, the yielding of the end-plate will first develop, which limits the action from the beam end to the beam-to-column joint and mitigates the damage within the joint zone of the steel rectangular tube column with blind bolts.

In this study, four different types of steel beam-to-rectangular hollow section column joints with blind bolts and end-plate yielding first are designed and experimentally studied. The effects of the steel beam with or without the composite concrete slab and rectangular steel tube column with or without infill concrete on the behavior of the beam-to-column joints under cyclic bending moments are investigated. The test results are summarized and may be used as a design guide for its application in practice.

2. Experimental program

2.1. Specimen preparation

The research objective is to identify the behavior of joints of steel beams to steel rectangular tube columns connected by blind bolts with flush end-plates. Four blind bolted flush end-plate joints to connect steel I-beams ($h \times b \times l \times t_w$ = 300×150×12×12 mm) with square CFST columns (side length = 200 mm and thickness = 12 mm) are designed. The thickness of the end-plate is 6 mm, making the end-plate the weakest element of the joint compared with the column tube wall and the blind bolts under bending due to gravity or earthquakes. In terms of the types of beams (pure steel beam and composite steel beam with concrete slab) and columns (pure steel tube columns and steel tube concrete-filled columns with rectangular section), a total of four different combinations of joints are prepared, as shown in Table 1 and Fig. 6. In Table 1, the first letter of the specimen label T represents the rectangular steel tube column and C represents the rectangular concrete-filled steel tube column. The second letter of the specimen label B represents the pure steel beam and C represents the full shear connection composite beam.

Table 1
Summary of joint specimens

Specimens	Column type	Beam type
TB	steel tube column	pure steel beam
TC	steel tube column	composite beam
CB	concrete-filled steel tube column	pure steel beam
CC	concrete-filled steel tube column	composite beam

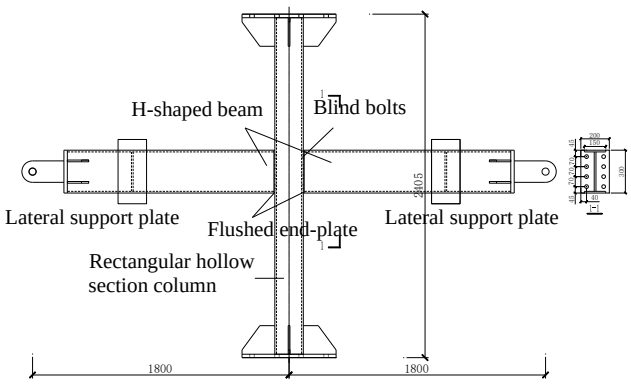

(a) Specimen TB

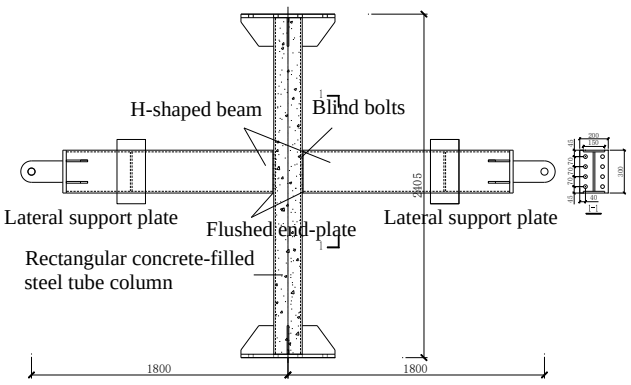

(b) Specimen CB

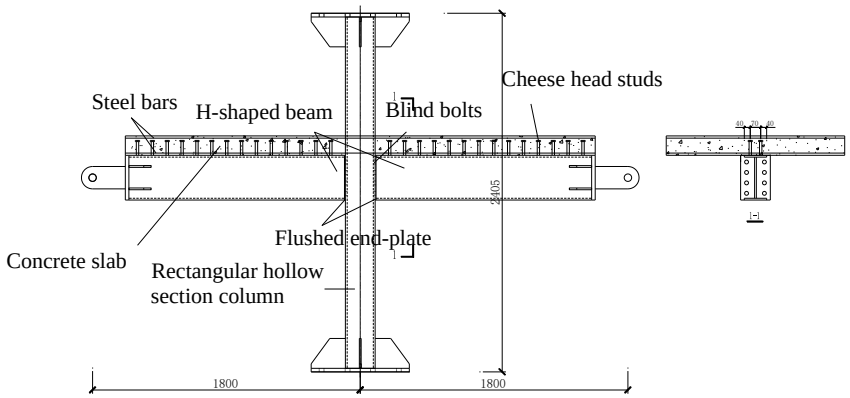

(c) Specimen TC

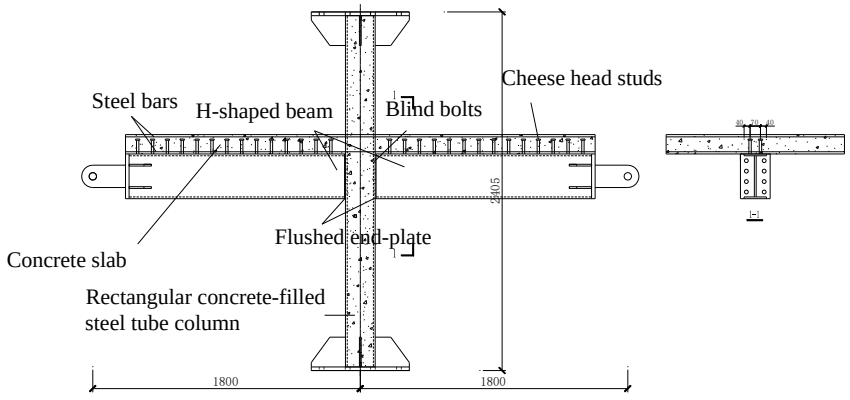

(d) Specimen CC

Fig. 6 Details of joint specimens (unit: mm)

2.2. Material properties

According to Chinese specification GB/T 228-2002[29], the mechanical properties of structural steels (elastic modulus E_s, yield strength f_y, ultimate strength f_u and elongation at fracture δ) used in the specimens are tested and summarized in Table 2. The concrete is prepared to achieve a nominal cubic strength of 40 MPa at 28 days. The mix proportion of concrete is water: cement: sand: aggregate = 0.54: 1.00: 1.30: 2.60. At the time of testing, the cubic strength and modulus of elasticity of concrete were 43.35 MPa and 35670 MPa, respectively. The reinforcement used in the test is HRB400 with a diameter of 8mm and a tensile strength of 592.49 MPa. The 8.8-NBB16 blind bolts are used in the test, and their tensile bearing capacity, shear bearing capacity and tensile stiffness are summarized in Table 3.

Table 2
Mechanical properties of structural steels

Thickness (mm)	Yield strength f_y (MPa)	Tensile strength f_u (MPa)	Elastic modulus E (GPa)	Elongation Δ (%)
6	345.72	501.36	204.82	33.66
12	387.60	520.02	194.52	37.08
25	396.04	503.94	211.02	43.36

Table 3
Mechanical properties of bolt

Bolt	Tensile bearing capacity (kN)	Shear bearing capacity (kN)	Tensile stiffness (kN/mm)
8.8-NBB16	161.13	278.89	131.98

2.3. Test setup

The test setup is shown in Fig. 7. The universal ball hinges are adopted at the top and bottom of the column of the specimens to simulate the zero moment condition at the point of contraflexure. An oil pressure actuator with 1000 kN loading capacity is used to apply the axial pressure at the top of the column, and the horizontal support is set between the column top steel base and the reaction frame to bear the horizontal reaction force from the column top. The beam end is hinged with the actuator, and the vertical load is applied at the beam end through the actuator with 500 kN loading capacity. For pure steel beam joints, the lateral support plates are welded on both sides of the steel beam, and the lateral support with rollers is arranged to restrict the out-of-plane displacement of the specimen during loading. For composite beam joints, the reaction frame is leaning against the side wall of the floor slab, which also limits the out-of-

plane displacement of the specimen.

(a) Test setup for specimens TB and CB

(b) Test setup for specimens TC and CC

Fig. 7 Test setup

The loading process is divided into three stages: (1) The pre-load with ±1mm displacement in the horizontal direction is applied to ensure that acquisition equipment works properly. (2) The actuator is used to apply the axial pressure to the square steel pipe column to the predetermined value (axial compression ratio = 0.15) and keep it constant throughout the test. (3) Finally, the vertical load is applied at two ends of the beam through the actuator. In the cyclic loading process, a lateral cyclic load is applied at the beam end, and the loading protocol is determined according to AISC 341-10[30], as plotted in Fig. 8.

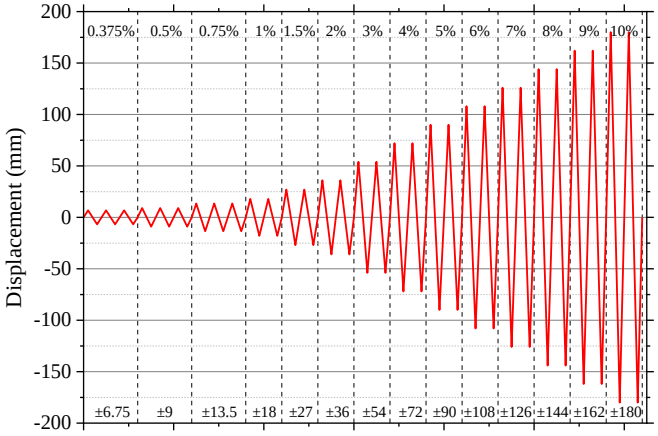

Fig. 8 Loading protocol

2.4. Measurements

To measure the local strains and displacements of joints, 79 strain gauges and 10 LVDTs are placed at critical locations of the beam, tube end plates and slab, as shown in Fig. 9.

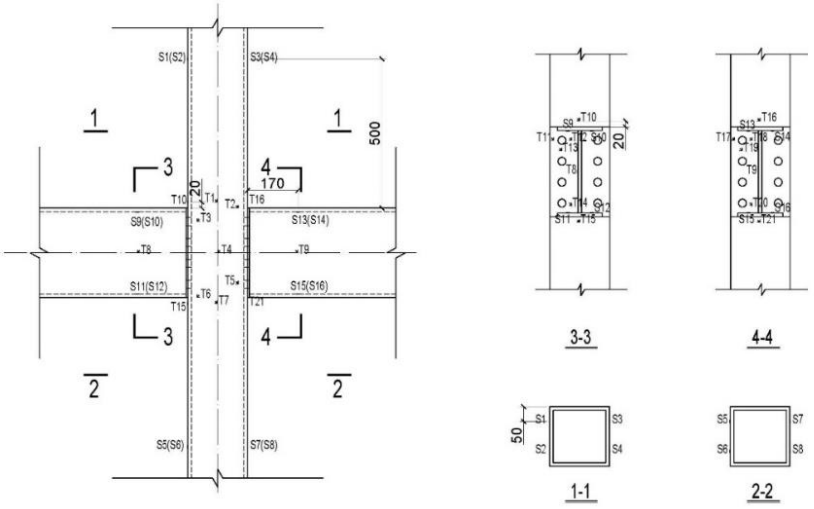

(a) Strain gauges for specimens TB and CB

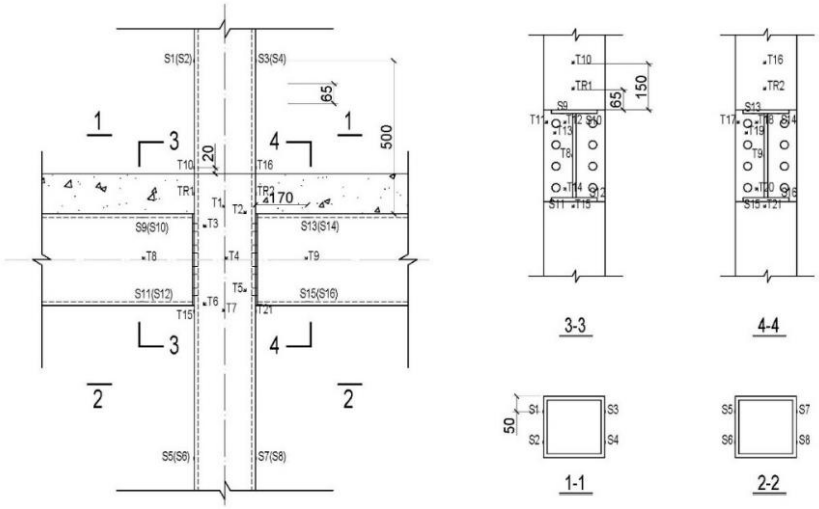

(b) Strain gauges for specimens TC and CC

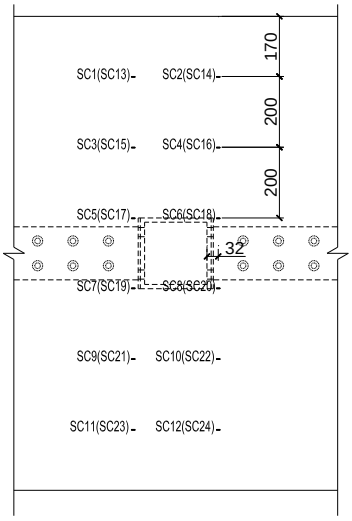

(c) Strain gauges for concrete slab

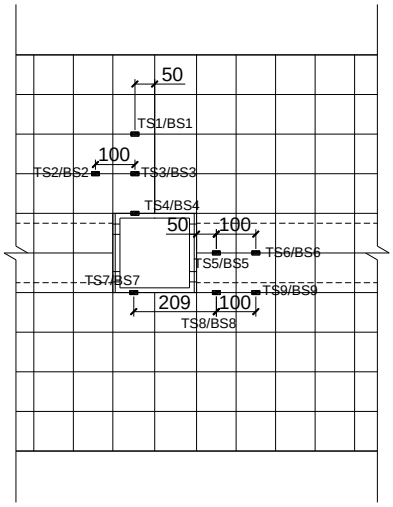

(d) Strain gauges for steel bars

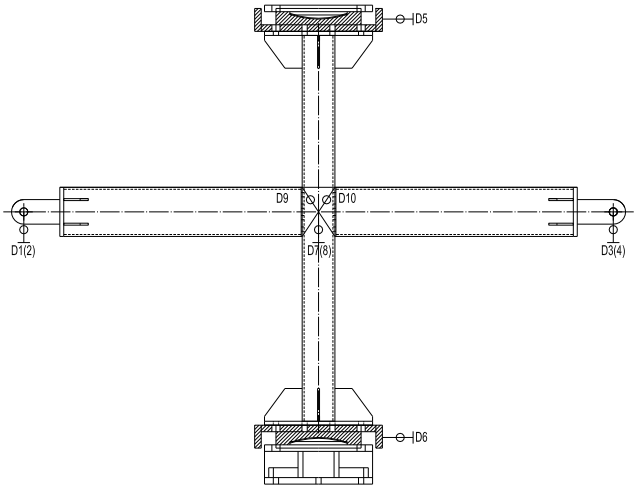

(e) LVDTs

Fig. 9 Arrangement of LVDTs and strain gauges (unit: mm)

In this test, the vertical displacement of the beam end is the key measurement object. The following five types of deformation shown in Fig. 10 can cause vertical deformations of the beam end. Only type (5) is the characteristic deformation of the joints itself, so the vertical displacement measured based on the beam end displacement meter needs to be deducted from the previous four types.

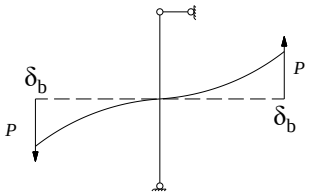

(1) Bending of beam

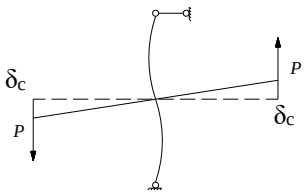

(2) Bending of column

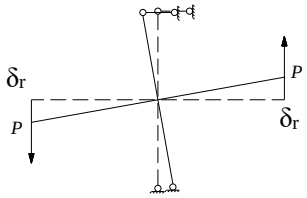

(3) Rigid body rotation

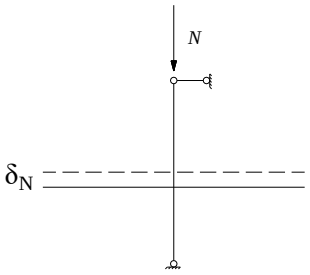

(4) Axial deformation of column

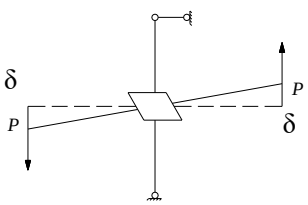

(5) Deformation of panel zone

Fig. 10 Deformation of beam-column joint

3. Test results

3.1. Typical phenomena

Typical phenomena that occurred during the tests on four joints are shown in Table 4 and Fig. 11. The story drift angles of each joint specimen corresponding to the above phenomena are summarized in Table 5.

Table 4
Typical phenomena of the joints in tests

ID	Phenomenon
A	The end-plate starts to yield
B	The column wall starts to yield
C	The first crack in the slab develops
D	A large number of floor cracks occur
E	The cracks penetrate between the upper and lower flanges of the slab
F	The floor concrete is crushed and hunched up
G	Falling of concrete block of the floor slab occurs
H	Exposed rebars in floor slab are observed
I	The topmost blind bolt loses pre-tension
J	The plasticity of blind bolt is deepened
K	Bending deformation of end-plate occurs
L	A crack on end-plate is observed
M	The crack penetrates in the thickness direction of the end plate
N	The end-plate and steel beam flange are completely torn at the crack
O	The end-plate crack develops vertically along the web of the steel beam
P	The column wall is inwardly concave and outwardly bulging

Table 5
Story drift angles corresponding to the phenomena listed in Table 4

Story drift ratio	Specimens			
	TB	TC	CB	CC
0.375%		B, C		
0.5%	A	A	A	A, B
0.75%				C
1%				
1.5%		D		
2%		B, J		
3%	J, K	G	K	
4%		L	L	F, G, I
5%	L	M, P		D, K
6%	M	F, H	M, N	E, L, H
7%		O	J	M, O
8%				
9%				
10%	N, O		O	

(a) Cracks penetrate between the upper and lower flanges of the slab

(b) The floor concrete is crushed and hunched up

(c) Falling of concrete block of floor slab

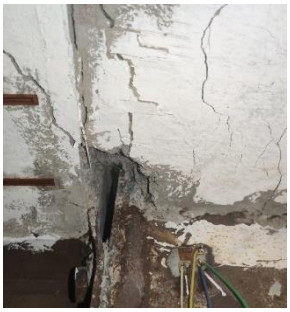

(d) Exposed rebars in floor slab

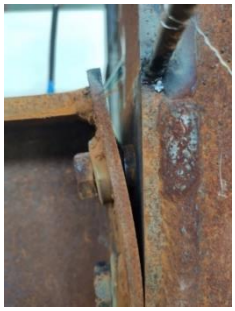

(e) Blind bolt loses pre-tension

(f) The plasticity of blind bolt is deepened

(g) Bending deformation of end plate

(h) Crack on end plate

(i) The crack penetrates in the thickness direction of the end plate

(j) The end-plate and steel beam flange are completely torn at the crack

(k) The end-plate crack develops vertically along the web of the steel beam

(l) The column wall is inwardly concave and outwardly bulging

Fig. 11 Typical phenomena of the joints in tests

3.2. Failure modes

The failure mode of the four joint specimens is the yield of the end-plate followed by fracture. When the interstory displacement angle reaches 4%, the cracks begin to appear on the end-plate of the four joints, then the crack extends to the penetration along the thickness direction of the end-plate and extends to the web of the H-shaped steel beam along the width direction of the end-plate, resulting in the tearing of the H-shaped steel beam from the end-plate. Finally, the bending moment cannot be transmitted from the H-shaped steel beam to the joint, resulting in failure. In order to avoid the joint failure mode in which the column wall is damaged before the beam end, which is highly unfavorable to the vertical bearing capacity of the column, the joint specimens in this paper are all designed to fail by end-plate yielding.

For composite beam joints with concrete floor (joint TC and CC), the floor slab cracks in tension and collapses in compression. In addition, due to the combined action of floor slabs, the column walls yield in these two joints. In particular, the column wall flange of joint TC is squeezed by the steel beam flange in the later stage of loading, resulting in obvious inward deflection and the column wall web buckling. On the contrary, the column walls of the other two joints remain elastic during loading.

The blind bolts of the four joint specimens were not fractured during the loading process. The H-shaped steel beam remained elastic, and no local buckling was found.

In summary, the failure modes of the four test specimens in the test can be divided into two types: end-plate fracture (TB and CB as shown in Fig. 11(h)-(k)), and a mixed mode of end-plate fracture, cracking and crushing of concrete slab and column wall yielding (TC and CC as shown in Fig. 11(a)-(d) and (h)-(l)).

3.3. Moment-Rotation curves

The bending moment M_0, right side and left side rotation angles θ_e and θ_w of the joints are calculated according to Eq. (1)-(5), where P is the load at the beam end; l_x=1694 mm is the distance between the loading point at the beam end and the outer edge of the end plate; δ_e and δ_w are respectively the beam end displacements caused by the deformation of the right side and left side joints; δ_1-δ_4 are respectively the readings of LVDTs D1-D4; and δ_b, δ_c, δ_r and δ_N are the vertical deformation of the beam end caused by various factors as shown in Fig. 10.

$$M_0 = Pl_x \tag{1}$$

$$\theta_e = \frac{\delta_e}{l_x} \tag{2}$$

$$\theta_w = \frac{\delta_w}{l_x} \tag{3}$$

$$\delta_e = \frac{1}{2}(\delta_1 + \delta_2) - \delta_b - \delta_c - \delta_r + \delta_N \tag{4}$$

$$\delta_w = \frac{1}{2}(\delta_3 + \delta_4) - \delta_b + \delta_c + \delta_r + \delta_N \tag{5}$$

The bending moment against rotation angle are plotted in Fig. 12. The bending moment-rotation curves of the four joints have the following characteristics:

(1) Since the sleeve part of the blind bolt has entered plasticity after installation, the hysteretic curve of the joint presents nonlinear characteristics from the beginning of loading.

(2) The bending capacity of the second circle of each load stage of the joint decreases to a certain extent compared with that of the first circle and increases with the increase of the interstory displacement angle. The reasons are as follows: with the increase of the interstory displacement angle, the plasticity of the blind bolt, especially the sleeve component, is significantly deepened. When the interstory displacement angle of a particular stage is loaded reversely, the blind bolt can no longer fit the end plate and return to its original position because it enters plasticity, demonstrating the phenomenon of separation from the end-plate. When the second circle of interstory displacement angle is positively loaded, the end-plate cannot make contact with the blind bolt properly within a specific range, resulting in the reduction of the second circle of flexural bearing capacity.

(3) The joint shows that the slope of the curve is considerably low in the middle range of each stage of loading, but the slope increases sharply at both ends. As a result, the hysteretic curve of each joint shows an inverted Z shape.

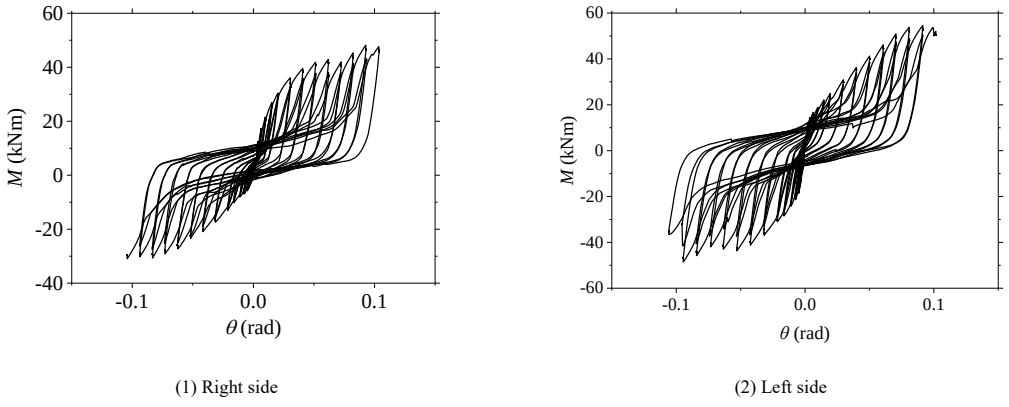

(1) Right side (2) Left side

(a) TB

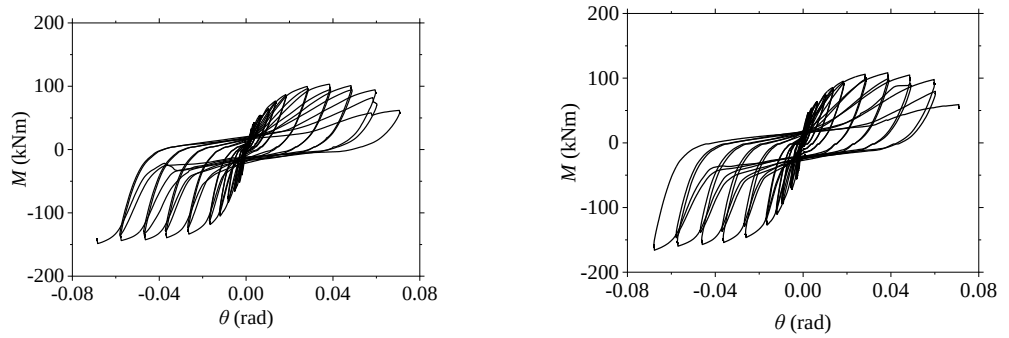

(1) Right side (2) Left side

(b) TC

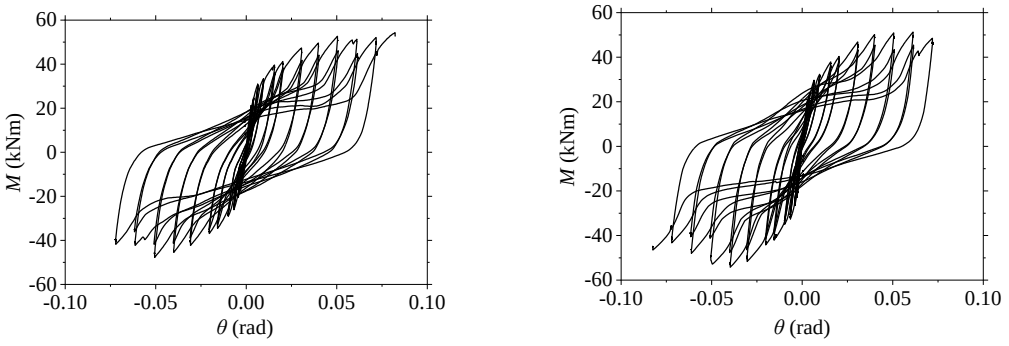

(1) Right side (2) Left side

(c) CB

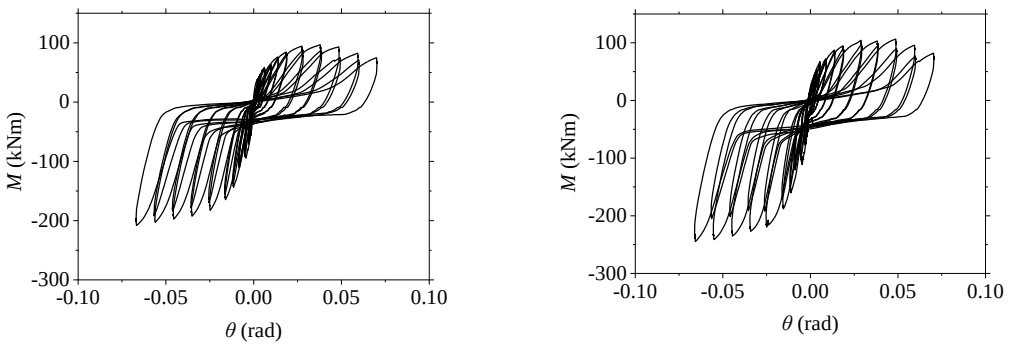

(1) Right side (2) Left side

(d) CC

Fig. 12 Moment – rotation hysteretic curves

4. Discussion

4.1. Skeleton curve and bending capacity

The skeleton curves of 4 joints are summarized as shown in Fig. 13. It can be seen from the skeleton curve of the joint that the bending moment of the pure steel joint and the full shear composite joint increases with the rotation angle until the end plate is torn, reducing the bearing capacity of the joint.

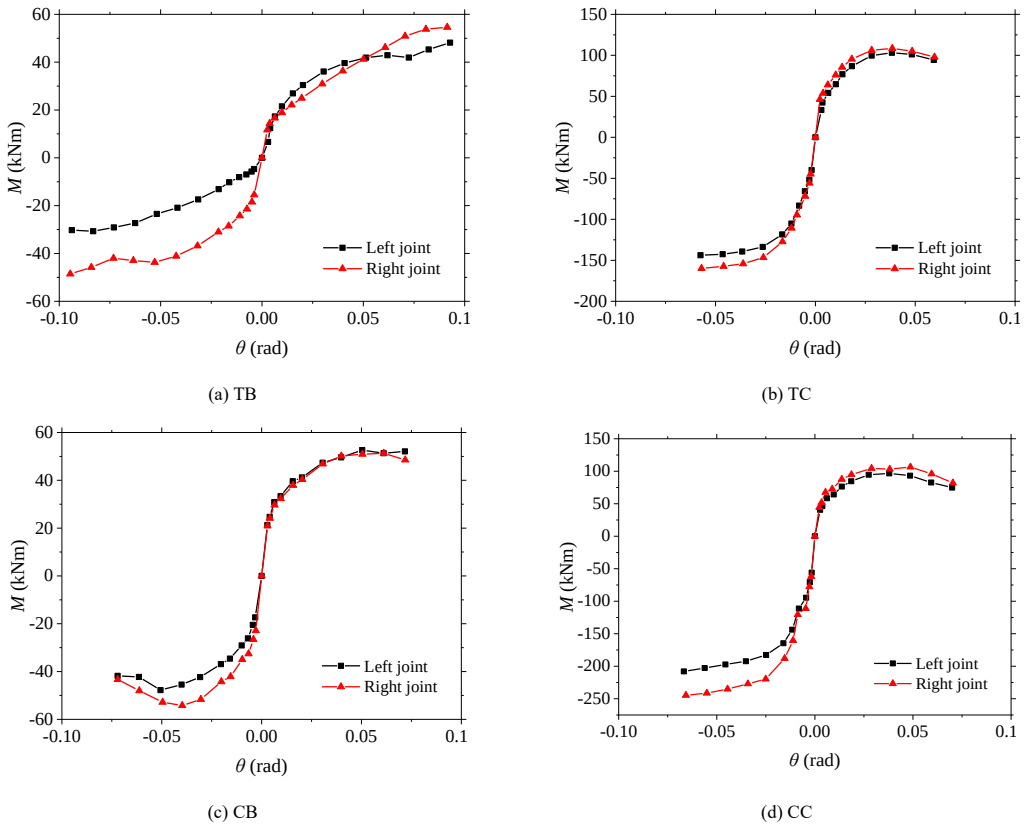

Fig. 13 Skeleton curves

According to the skeleton curve of each joint obtained, the maximum bending moments in the skeleton curve are taken as the bending capacities of the joints under the action of positive and negative bending moments. See Table 6 for the summary.

Considering that not all parts of the specimen reach their failure modes during loading, the maximum bending moment is not the ultimate bending capacity of the joint. Therefore, for each joint, the maximum values under the positive and negative bending moments are taken as its bending capacities as shown in Table 7. According to Eurocode 3[31], TC and CC are partial-strength joints, and TB and CB are hinge joints with negligible moment resistance.

Table 6
Bending capacity of each joint specimen in tests

Specimen	Right side		Left side	
	Sagging moment (kN·m)	Hogging moment (kN·m)	Sagging moment (kN·m)	Hogging moment (kN·m)
TB	48.16	30.70	54.61	48.57
TC	103.13	143.82	108.48	159.86
CB	52.65	47.77	51.29	54.21
CC	96.68	207.99	106.48	244.75

Table 7
Test value of bending capacities of joints

Specimen	Bending capacity (kN·m)	
	Sagging bending	Hogging bending
TB	54.61	48.57
TC	108.48	159.86
CB	52.65	54.21
CC	106.48	244.75

4.2. Initial rotational stiffness

For four joints in this test, the initial rotational stiffness under the action of positive and negative bending moments is different, so the initial rotational stiffness is calculated for the action of positive bending moment and negative bending moment, respectively.

Taking the load F_1 and displacement X_1 corresponding to the peak point of the bending moment angle curve after the first level interstory displacement angle loading is completed (0.375%), and the initial rotational stiffness of the joint is calculated according to Eq. (6)[31]. The summary is shown in Table 8.

$$K_1 = \frac{|F_1|}{|X_1|} \tag{6}$$

Table 8
Initial rotational stiffness of each joint specimen in tests

Specimen	Initial rotational stiffness (kN·m /rad)			
	Right side		Left side	
	Sagging bending	Hogging bending	Sagging bending	Hogging bending
TB	2198	1201	4395	4076
TC	11130	21176	20409	19006
CB	7362	5418	7005	7858
CC	15087	34829	19405	33517

Referring to the method defining the bending capacity of the joints, the maximum value of the initial rotational stiffness of each type of joints obtained by the test is also calculated, as summarized in Table 9.

Table 9
Test value of initial rotational stiffness of joints

Specimen	Initial rotational stiffness (kN·m/rad)	
	Sagging bending	Hogging bending
TB	4395	4076
TC	20409	21176
CB	7362	7858
CC	19405	34829

In this test, the loading mode of the joint is beam loading, which belongs to a non-sway frame. According to the formula of Eurocode 3[31], the stiffness of the hinge connection K_p is 2738 kN·m/rad and the stiffness of the rigid connection K_r is 43817 kN·m/rad, which can be respectively calculated by Eqs. (7) and (8), where E is the elastic modulus of steel; I_b is the second moment of inertia of the steel beam around the principal major axis and L_{b0} is the span of the steel beam.

$$K_p = \frac{0.5EI_b}{L_{b0}} \tag{7}$$

$$K_r = \frac{8EI_b}{L_{b0}} \tag{8}$$

According to the classification method by initial rotational stiffness in Eurocode 3[31], the four joints in this test are semi-rigid joints.

4.3. Ductility

The ductility coefficient of the joint is calculated according to Specification for seismic test of buildings (JGJ/T 101-2015)[32] given by

$$\mu = \frac{\theta_u}{\theta_y} \tag{9}$$

where θ_u and θ_y are respectively the ultimate deformation and yield deformation.

The definition of ultimate deformation and yield deformation of the joint is presented in Fig. 14[32]. The curve is the skeleton curve of each joint under positive and negative bending moments. The abscissa corresponding to the intersection of the straight line with the slope of the origin as the initial rotational stiffness and the horizontal line with the value of the ultimate bending moment is taken as the yield deformation of the test specimen. The abscissa corresponding to the curve point to which the bending moment of the test specimen is reduced is taken as the ultimate deformation of the test specimen. If the test specimen is not loaded to failure, the rotation angle at the loading stop time is taken as the ultimate deformation. The M_u represents the maximum bending moment obtained from moment-rotation curve. According to Specification for seismic test of buildings (JGJ/T 101-2015)[32], the rotation corresponding to bending moment equals to $0.85\times M_u$ is defined as the ultimate deformation in the present study. The yield displacement, ultimate displacement and ductility coefficient of each joint under the action of positive and negative bending moments are calculated and summarized in Table 10 and Table 11.

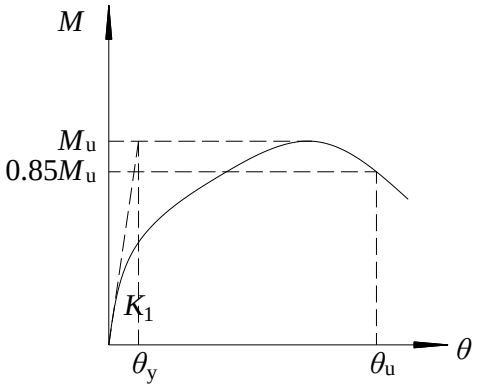

Fig. 14 Calculation method of ultimate deformation and yield deformation of joints[32]

Table 10
Ductility coefficient of each joint specimen (Right Side)

Specimen	Sagging bending			Hogging bending		
	θ_y (mrad)	θ_u (mrad)	μ	θ_y (mrad)	θ_u (mrad)	μ
TB	21.91	92.80	4.24	25.56	93.81	3.67
TC	9.27	38.33	4.14	6.79	57.52	8.47
CB	7.15	50.39	7.05	8.82	50.60	5.74
CC	6.41	37.92	5.92	5.97	66.77	11.18

Table 11
Ductility coefficient of each joint specimen (Left Side)

Specimen	Sagging bending			Hogging bending		
	θ_y (mrad)	θ_u (mrad)	μ	θ_y (mrad)	θ_u (mrad)	μ
TB	12.43	91.39	7.35	11.91	94.55	7.94
TC	5.32	38.55	7.25	8.41	56.98	6.77
CB	7.32	61.17	8.35	6.90	39.73	5.76
CC	5.49	48.71	8.88	7.30	65.70	9.00

It can be concluded that:

(1) The negative bending ductility of full shear composite joints is better than the positive bending ductility.

(2) The ductility coefficient of the rectangular steel tube column joint is close to that of the rectangular concrete-filled steel tube column joint, indicating that the type of column has a negligible effect on the ductility coefficient of the joint.

(3) American seismic code for steel structures (AISC 341-10)[30] stipulates that when the moment bearing capacity of the joint against earthquake drops to 80%, the interstory displacement angle shall not be less than 0.04 rad. Except for the composite steel beam-to-column joint, all other types of joints demonstrate excellent ductility with the interstory displacement angle greater than 0.04 rad, which meets the requirement for resisting severe earthquakes.

4.4. Influence of different structures on joint performance

The influences of the types of columns and beams on hysteretic behavior of joints are studied in this section. The skeleton curves of four joints are plotted in Fig. 15. It is observed that both the moment bearing capacity and initial rotational stiffness of composite steel beam joints with concrete slab are much higher than those of pure steel beam joints, whether the rectangular steel tube column is filled with concrete.

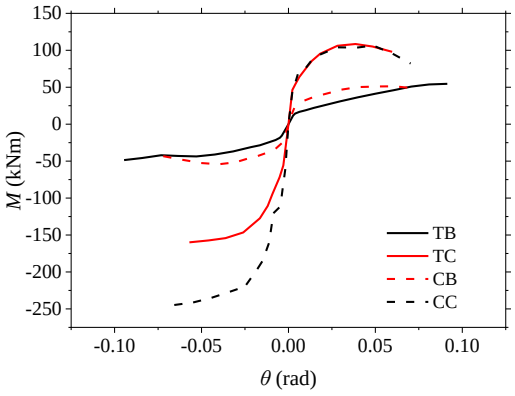

Fig. 15 Comparison of skeleton curves among four joints

For pure steel beam joints (TB and CB), it is observed that (1) The moment bearing capacities of these two joints are close. (2) The initial rotational stiffness of the joint with concrete in the column (CB) is slightly larger than that of the joint without concrete in the column (TB). It is because the failures of these two joints are both end-plate fracture. Therefore, whether concrete is in the column has negligible influence on moment bearing capacity and initial rotational stiffness.

For composite beam joints (TC and CC), it is observed that (1) The positive moment bearing capacity and positive initial rotational stiffness of these two joints are the same. (2) The negative moment bearing capacity and negative initial rotational stiffness of the joint with concrete in the column (CC) are both larger than those without concrete in the column (TC). The reasons are as follows: Under the positive bending moment, the concrete floor bears compression and the blind bolts bear tension. Therefore, whether concrete is in the column has negligible influence on the moment bearing capacity and initial rotational stiffness. However, under the negative bending moment, the reinforcements in the concrete plate bear tension and the column bears compression. Without concrete in the column, the column wall deforms significantly and enters into plasticity. On the contrary, the compression is transmitted to the concrete in the column through the column wall. Thus, the moment bearing capacity is greatly improved.

5. Conclusion

Based on the experimental investigation on the cyclic behavior of the joints for steel H-shaped beam to steel rectangular tube column connected by blind bolts with end-plate, the following conclusions can be drawn:

(1) With appropriate design, the failure mode of all the joint specimens is yielding of end-plate, which is beneficial to limit the action at the beam end transferred to the column and mitigate the failure of the column zone in the beam-to-column joint leading more severe damages to structures. The fracture will not happen on the end plate if the story-drift ratio is less than 4%.

(2) For composite beam joints, concrete in the joint core was cracked and crushed. As a result, the column wall yielded or even inwardly deflected due to its combined effect, which is not observed in pure steel beam joints.

(3) All the types of joints in this study can be classified as semi-rigid according to the criteria given in Eurocode 3. However, due to the contribution of the concrete slab, the bending capacity and initial rotational stiffness of the entire composite joints are significantly greater than those of the pure steel joints, whether under the action of sagging or hogging moments.

(4) Except for the composite beam joint under the action of positive bending moment, all the joints demonstrate excellent ductility with the interstory displacement angle greater than 0.04 rad, which satisfies the requirement for resisting severe earthquakes.

Acknowledgement

The research work presented hereinabove was supported by the National Key Research and Development Program of China (Project No. 2016YFC0701204).

References

[1] Wang HH, Cao FH. Research on Properties for Semi-Rigid Connections of H-Section Beam and RHS Column. Building Science. 2009.
[2] Miller DK. Lessons learned from the Northridge earthquake. ENG STRUCT. 1998.
[3] Tremblay R, Filiatrault A, Bruneau M, Nakashima M, Prion H, Devall R. Seismic design of steel buildings: lessons from the 1995 Hyogo-ken Nanbu earthquake. CAN J CIVIL ENG. 1996;23727-56.
[4] Lindapter International Ltd, Type HB Hollo-bolt for Blind Connection to Structural Steel and Structural Tubes, Lindapter International Ltd., UK, 1995. <http://www.lindapter.com>.
[5] ZHANG, J., Research on mechanical properties of domestic self-lock one-side bolt. 2016, Tongji University: Shanghai, China [in Chinese] [.
[6] JIANG Y, LI G, CHEN C, et al. Experimental study on tensile behavior of blind bolt[J]. ce/papers, 2021,4(2-4): 100-109.
[7] Eldin A. Behaviour of Blind Bolted Moment Connections for Square HSS Columns. Concept Development. 1993.
[8] Korol R M, Ghobarah A, Mourad S. Blind bolting W-shape beams to HSS columns[J]. Journal of Structural Engineering, 1993, 119(12): 3463-3481.
[9] France J E, Davison J B, Kirby P A. Strength and rotational stiffness of simple connections to tubular columns using flowdrill connectors[J]. Journal of Constructional Steel Research, 1999, 50(1):15-34.
[10] France JE, Davison JB, Kirby PA. Moment-capacity and rotational stiffness of endplate connections to concrete-filled tubular columns with flowdrilled connectors. J CONSTR STEEL RES. 1999;5035-48.
[11] Barnett TC, Tizani W, Nethercot DA. The practice of blind bolting connections to structural hollow sections: A review. STEEL COMPOS STRUCT. 2001;11-16.
[12] Barnett T, Tizani W, Nethercot D A. Blind bolted moment resisting connections to structural hollow sections[J]. Connections in steel structures, 2000, 4.
[13] Elghazouli AY, Malaga-Chuquitaype C, Castro JM, Orton AH. Experimental monotonic and cyclic behaviour of blind-bolted angle connections. ENG STRUCT. 2009;312540-53.
[14] Liu Y, Málaga-Chuquitaype C, Elghazouli AY. Response and component characterisation of semi-rigid connections to tubular columns under axial loads. ENG STRUCT. 2012;41510-32.
[15] Lee J, Goldsworthy HM, Gad EF. Blind bolted T-stub connections to unfilled hollow section columns in low rise structures. J CONSTR STEEL RES. 2010;66981-92.
[16] Lee J, Goldsworthy HM, Gad EF. Blind bolted moment connection to sides of hollow section columns. J CONSTR STEEL RES. 2011;671900-11.
[17] Wang J, Zhang N. Performance of circular CFST column to steel beam joints with blind bolts. J CONSTR STEEL RES. 2017;13036-52.
[18] Wang J, Zhang N, Guo S. Experimental and numerical analysis of blind bolted moment joints to CFTST columns. THIN WALL STRUCT. 2016.
[19] Wang J, Zhang H, Jiang Z. Seismic behavior of blind bolted end plate composite joints to CFTST columns. THIN WALL STRUCT. 2016;108256-69.
[20] Wang J, Li B, Wang D, Zhao C. Cyclic testing of steel beam blind bolted to CFST column composite frames with SBTD concrete slabs. ENG STRUCT. 2017.
[21] Guo L, Wang J, Wang W, Duan M. Seismic evaluation and calculation models of CFDST column blind bolted to composite beam joints with partial shear interaction. ENG STRUCT. 2019;196109261-9.
[22] Wang J, Guo L, Guo X, Ding Z. Seismic response investigation on CFDST column to steel beam blind-bolted connections. J CONSTR STEEL RES. 2019;161137-53.
[23] Wang J, Chen L, Han L. Static and Seismic Experiments and Analysis Models of Blind Bolted end Plate Joints to CFT Columns. Shanghai International Conference on Technology of Architecture & Structure2009.
[24] Wang J, Spencer BF. Experimental and analytical behavior of blind bolted moment connections. J CONSTR STEEL RES. 2013;8233-47.
[25] Wang J, Lin Z, Jr B. Seismic response of extended end plate joints to concrete-filled steel tubular columns. ENG STRUCT. 2013;49876-92.
[26] Guo L, Wang J, Wang W, Wang C. Cyclic tests and analyses of extended endplate composite connections to CFDST columns. J CONSTR STEEL RES. 2020;167105937.
[27] LI M., Research on cyclic behavior and design method of hollow section column-to-beal connections with siip-critical blind bolts. 2017, Tongji University: Shanghai, China [in Chinese].
[28] Jiao W, Wang W, Chen Y, Teh LH. Seismic performance of concrete-filled SHS column-to-beam connections with slip-critical blind bolts. J CONSTR STEEL RES. 2020;170106075.
[29] GB/T 228-2002. Code for acceptance of construction quality of steel structures. Beijing: General Administration of Quality Supervision, Inspection and Quarantine of the People's Republic of China; 2002 [in Chinese].
[30] American Institute of Steel Construction. ANSI/AISC 341-10: Seismic Provisions for Structural Steel Buildings[S]. 2010.
[31] European Committee for Standardization. EN 1993-1-8: 2005, Eurocode 3: Design of steel structures - Part 1-8: Design of joints[S]. 2005.
[32] JGJ / T 101-2015. Specification for seismic test of buildings. Beijing: Ministry of Housing and Urban-Rural Construction of the People's Republic of China; 2015 [in Chinese].